

GEOLOGY

What sets river width?

Kieran B. J. Dunne^{1,2,*} and Douglas J. Jerolmack^{2,3}

One of the simplest questions in riverine science remains unanswered: “What determines the width of rivers?” While myriad environmental and geological factors have been proposed to control alluvial river size, no accepted theory exists to explain this fundamental characteristic of river systems. We combine analysis of a global dataset with a field study to support a simple hypothesis: River geometry adjusts to the threshold fluid entrainment stress of the most resistant material lining the channel. In addition, we demonstrate how changes in bank strength dictate planform morphology by exerting strong control on channel width. Our findings greatly extend the applicability of threshold channel theory, which was originally developed to explain straight gravel-bedded rivers with uniform grain size and stable banks. The parsimonious threshold-limiting channel model describes the average hydraulic state of natural rivers across a wide range of conditions and may find use in river management, stratigraphy, and planetary science.

INTRODUCTION

What controls the width of a river? Despite the need for channel design principles in river management and restoration, the robust scaling relations observed between channel shape and discharge, and the rapid development of sophisticated numerical models that simulate landscapes, this fundamental question remains unanswered (1). Channels initiate spontaneously when water flows over an erodible, granular medium (2, 3). With a constant water flux, erosion widens the channel until eventually the fluid shear stress everywhere along the boundary, τ_b , is equal to the threshold for particle entrainment, τ_c (4). The solution for the stable geometry (i.e., width and depth) of a threshold channel is well known and forms the basis for canal design (5). Natural alluvial rivers, of course, differ significantly from canals. Because of the sediment loads and range of floods imposed on them, rivers ceaselessly remold the channel (6, 7)—dynamics that can be reproduced in laboratory experiments (8–11). Parker (6) proposed a mechanistic solution for the bankfull geometry of an idealized model system: a straight and trapezoidal channel with stable (noneroding) banks, lined with uniform coarse (gravel) material. The key component of his model was the explicit treatment of turbulent diffusion, which determines the lateral stress profile across the channel. This allows for stable banks with $\tau_b \leq \tau_c$ while accommodating transport in the channel center where $\tau_b \approx 1.2\tau_c$ (Fig. 1C). The latter provides a closure scheme that, along with mass and momentum conservation for the fluid (Supplementary Materials), allows one to derive a simplified set of “regime equations” that predict the channel bankfull width, W_{bf} , and depth, H_{bf} (Fig. 1C), as functions of specified hydraulic variables

$$W_{bf} = \frac{Q_{bf} S}{C_f g^{1/2} \left(\frac{1.2 \tau_c}{\rho g} \right)^{3/2}} \quad (1)$$

and

$$H_{bf} = \frac{1.2 \tau_c}{\rho g S} \quad (2)$$

where Q_{bf} , S , C_f , g , and ρ are the bankfull discharge, slope, empirical friction factor (see eq. S3), acceleration due to gravity, and density of water, respectively (Fig. 1C; see Materials and Methods).

¹Department of Earth, Environmental, and Planetary Sciences, Rice University, Houston, TX 77005, USA. ²Department of Earth and Environmental Science, University of Pennsylvania, Philadelphia, PA 19104, USA. ³Department of Mechanical Engineering and Applied Mechanics, University of Pennsylvania, Philadelphia, PA 19104, USA. *Corresponding author. Email: dengjiamin@gmail.com

The applicability of a constant formative stress condition for natural rivers, which are subjected to a range of flood magnitudes, has led some to propose that a wide range of floods may be responsible for determining channel form (11–14). As a first step toward simplifying natural flow variability, Wolman *et al.* (15) proposed that the wide range of flows imposed on a fluvial system may be represented by a characteristic “bankfull” flood that, through its combination of recurrence frequency and magnitude, transports the most sediment over long time scales—and thus determines channel geometry. More recent analysis of global river databases provides strong support that river geometry is adjusted to a channel-forming fluid stress associated with bankfull flow (16, 17). Other studies have suggested that additional factors such as sediment supply, vegetation, and bank cohesion (resulting from a combination of factors such as clay content, sediment composition, root density, etc.), not considered in the original Parker model, must also play a role in determining the geometry of alluvial rivers (18–20). Nonetheless, the near-threshold closure has been shown to describe hydraulic geometry trends in natural gravel-bedded rivers (here defined as having a median bed sediment diameter, $D_{50} > 1$ cm) (4, 16, 17). Rivers with fine-grained ($D_{50} < 1$ cm) beds, however, do not follow the near-threshold condition. Bankfull flow conditions typically correspond to $\tau_{bf}/\tau_c > 1$, meaning that bed material sediment is also well suspended in the flow (21)—a condition that has been considered incompatible with stable, threshold banks.

Schumm (22) proposed that the geometry of these “suspension rivers” [cf. (23)] is in some way related to the composition of their channel banks, and provided empirical evidence that the channel aspect ratio (W_{bf}/H_{bf}) is inversely proportional to the amount of cohesive sediment in the banks of sand-bedded rivers (22, 24). Empirical correlations between channel geometry and bank composition have been elaborated on by subsequent authors (20, 25). Mechanistic theories developed to explain the geometry of fine-grained rivers—mostly by incorporating turbulent lateral transport of suspended sediment toward banks to balance inward lateral transport of bed load (26, 27)—have failed to capture observed hydraulic geometry trends. In the absence of a theory for the averaged channel geometry that is comparable to that of gravel-bedded rivers, a variety of heuristic channel closure schemes have been proposed and debated (19, 28). Recent research, however, has begun to compile evidence for similarities among near-threshold gravel-bedded rivers and suspension-dominated sand-bedded rivers. For example, the

Copyright © 2020 The Authors, some rights reserved; exclusive licensee American Association for the Advancement of Science. No claim to original U.S. Government Works. Distributed under a Creative Commons Attribution NonCommercial License 4.0 (CC BY-NC).

Downloaded from <http://advances.sciencemag.org/> on December 5, 2020

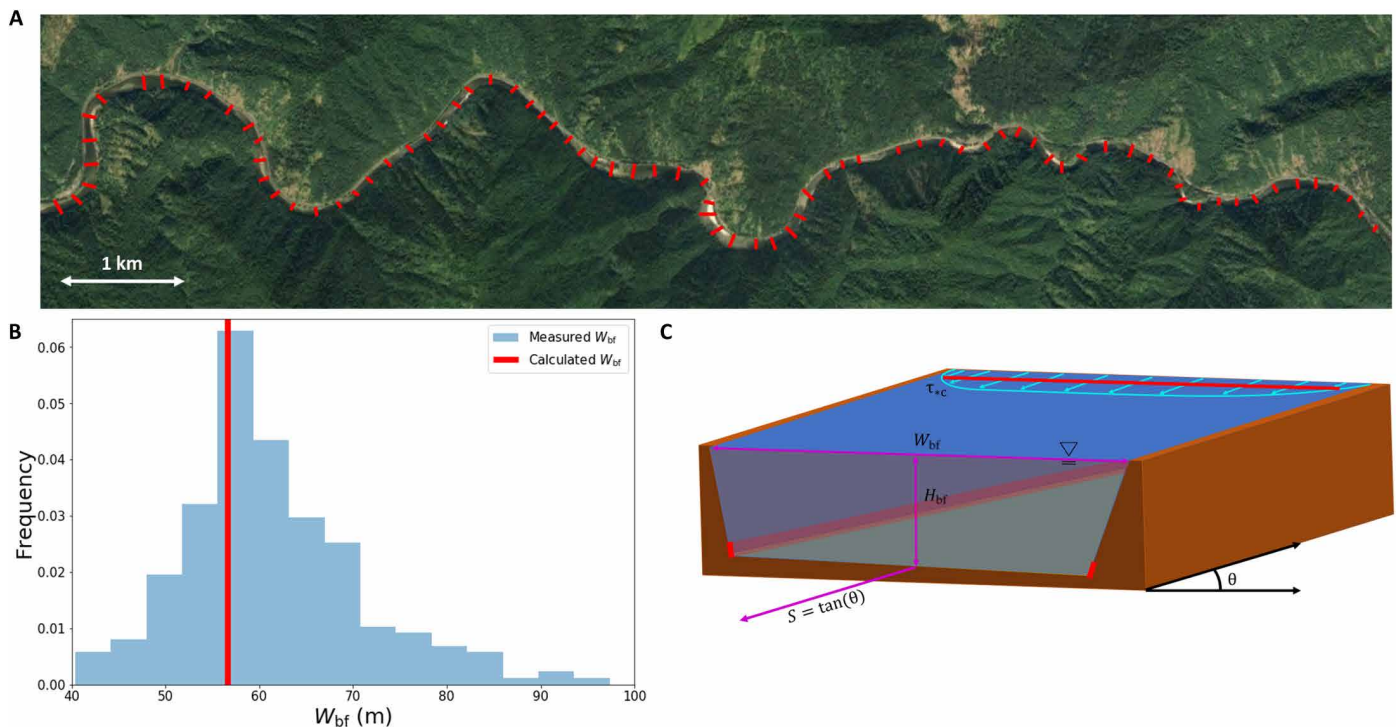


Fig. 1. Illustration of the mean field approximation of the threshold-limited channel model. (A) The Lochsa River, Idaho, USA. Red lines indicate approximately every third measured W_{bf} from Google Earth (image source: Google Earth). (B) Histogram of W_{bf} ($n = 230$). Red line indicates calculated W_{bf} from Eq. 1, which is in close agreement with the observed mode. Average channel width ($\langle W_{bf} \rangle = 61.4$ m, SD = 9.6 m, SE = 0.6 m). (C) Schematic of an idealized straight, trapezoidal channel. Cyan lines at the surface illustrate lateral boundary fluid shear stress profile across the channel, τ_{bf} . Red lines at the bank toe show the location where bed and bank materials meet. Horizontal red line intersecting the cyan velocity profile indicates τ_c of the threshold-limiting material. For the Parker model, $\tau_{bf} = \tau_c$ at the bank toe and $\tau_{bf} = 1.2\tau_c$ in the channel center.

hydraulic geometry scaling relations of sand-bedded rivers appear to follow those of gravel-bedded rivers, but with an offset. That offset can be reproduced with a model that assumes a constant, average formative shear stress that is much larger than the threshold value (29, 30). We have hypothesized that this deviation results due to a handoff from bed material-controlled hydraulic geometry to bank material-controlled hydraulic geometry (23), and proposed a generalization of the Parker closure that provides a theoretical explanation for the geometry of both coarse-grained and fine-grained alluvial rivers. Almost concurrently, Francalanci *et al.* (31) proposed a related model in which τ_c of riverbank (rather than bed) material—along with friction effects associated with drag on the banks—determines the hydraulic geometry of sand- and gravel-bedded rivers. We refer to the unification of the Parker closure and the Schumm postulate as the “threshold-limited channel” model. It states that river geometry adjusts to the threshold fluid entrainment stress of the most resistant material lining the channel perimeter. For gravel-bedded rivers, the entrainment threshold of bed sediment is larger than that of (likely) cohesive and/or vegetated riverbanks (23). Sand, however, has the lowest entrainment stress; typically cohesive and/or vegetated banks have substantially higher entrainment stresses than the bed. We posit that the cross-sectional geometry of fine-grained rivers is set by the threshold stress of cohesive bank-toe material, which forms the structural anchor of the riverbank (Fig. 1) (23). Unfortunately, published studies rarely, if ever, report estimates of τ_c for bank-toe material, because of the difficulty

of predicting and measuring the entrainment threshold of cohesive sediment (32). Thus, the threshold-limited channel model has not yet been tested.

In this study, we combine analysis of a global dataset of hydraulic geometry measurements, with a field study using a purpose-built device that measures the in situ entrainment threshold of bank-toe material, to test the threshold-limited channel model. In addition, we quantitatively show how changes in the entrainment threshold may drive transitions in river channel pattern—from braided to single threaded—by exerting a first-order influence on channel aspect ratio.

Parker theory: A mean field approximation for dynamic rivers

Given the dynamic nature of rivers, it is natural to be concerned about the application of a steady-state model—that predicts a static channel configuration—to dynamic, natural channels (whether sand or gravel bedded). Alternative formulations for channel geometry have been built around the concept of a dynamic equilibrium; the condition in which a stable average (although not static) channel geometry is actively maintained by the superposition of competing, dynamic processes. For example, a dynamic equilibrium theory for actively meandering channels has been proposed that models cohesive slump block failure and vegetation encroachment, both of which armor noncohesive sediment at the base of a cut bank and prevent the channel from overwidening (33). This model has also been extended to incorporate the role of overbank deposition of

sediment, which can compensate for sediment removal from floodplains due to channel migration; this allows both floodplains and channels to maintain a constant average morphology dynamically (33, 34). Validation and implementation of such a model, however, are reliant on a specific floodplain stratigraphy—i.e., cohesive sediment caps on top of noncohesive deposits—as well as the assumption of specific residence times of collapsed slump blocks in channels.

The assumptions of the Parker model (6) certainly appear to be incompatible with natural rivers that are typically sinuous, with heterogeneous bed and bank materials, and variable discharge, for which bank erosion and deposition are common. Yet, hydraulic geometry scaling relations describe the overall trends of alluvial rivers—if not the variability around those trends—without including any information about dynamics or variability within each river (35). Considering first the case of gravel-bedded rivers, we suggest that there are two factors that explain this apparent incompatibility. First is that gravel has a larger entrainment threshold than typical bank materials such as mud or sand (23); riverbank composition likely influences the rates and style of bank erosion (33), but not the overall channel size (36). Second is the idea that the lateral fluid stress profile in a straight channel is approximately equal to the spatially averaged flow over many cross sections in a curved channel. The uniform flow approximation for boundary stress—the so-called depth-slope product, $\tau_{bf} = \rho g H_{bf} S$ —can only be applied over length scales significantly larger than individual bends. As pointed out by Dietrich *et al.* (37), it is the lowest-order stress model. Higher-order behaviors like flow around bends produce stresses that vary spatially above and below the average. This allows erosion (deposition) on the outside (inside) of meander bends, as well as associated lateral grain size sorting and dynamic feedback between channel curvature and the flow field (38), while maintaining a stable channel geometry on average (37, 39). Thus, we propose that, in addition to being a direct model for the limited case of a static channel, the Parker theory is a “mean field approximation” that describes the time- and space-averaged geometry of natural, dynamic gravel-bedded rivers. We use the term mean field not in a strict statistical mechanics sense, but in a more general statistical physics parlance (40): The complex (many body) flow and sediment transport problem is reduced to an approximate interaction of the bed with an averaged shear stress. In this interpretation, the predicted static channel in the theory would represent a statistically expected state for a natural river; the model says nothing about the nature of variation around this expected state. To illustrate, we consider a reach of the Lochsa River, a gravel-bedded meandering river in Idaho ($Q_{bf} = 446 \text{ m}^3 \text{ s}^{-1}$, $D_{50} = 0.15 \text{ m}$, $S = 0.0023$, $\tau_c = 62.3 \text{ Pa}$) (16). Although there is significant spatial variation in measured channel width, the modal value is in close agreement with the Parker model, which approximates the river as a straight, trapezoidal channel with uniform grain size, constant discharge, and stable banks (Fig. 1.).

RESULTS

Analysis of a global dataset

Having demonstrated that dynamic gravel-bedded rivers are compatible with the Parker theory, we now pursue the generalization of the latter to the threshold-limited channel model. We note that this approach does not necessarily contradict the dynamic equilibrium model that invokes slump-block armored banks (34, 41); depending on the time scale required to erode these blocks, the relevant value

for τ_c could represent a time-integrated quantity that averages over cohesive (slump) and noncohesive (bank-toe) material. We examine a global dataset of river hydraulic geometry (16, 23, 28, 42) that spans a wide range of parameter space: $0.01 \leq D_{50} \leq 700 \text{ mm}$, $8.75 \times 10^{-6} \leq S \leq 0.35$, and $0.2 \leq Q_{bf} \leq 216,340 \text{ m}^3/\text{s}$. For gravel-bedded rivers ($D_{50} > 1 \text{ cm}$), we see that bankfull fluid stresses, τ_{bf} , calculated using the depth-slope product from bankfull hydraulic geometry, cluster around the entrainment threshold estimated from the Shields curve using the D_{50} of riverbed sediments (Fig. 2A). This is consistent with both theoretical predictions and the findings of numerous empirical studies (6, 16, 35). The substantial scatter is likely due to site-specific controls on τ_c that are not accounted for with the Shields estimate; the scatter in values of τ_{bf}/τ_c for gravel-bedded rivers is greatly reduced—from a factor of 10 to less than 2—when site-specific empirical measurements for τ_c are used (16, 17). For fine-grained rivers with $D_{50} < 1 \text{ cm}$, however, we see rivers peel off of the Shields curve; the smaller the riverbed grain size, the larger bankfull shear stress deviates from the threshold expectation (i.e., $\tau_{bf}/\tau_c \gg 1$) (4, 23).

Given the minimal uncertainty in grain size data, we infer that this departure, which occurs for bankfull shear stress values of the order $\tau_{bf} \sim 10^1 \text{ Pa}$, represents the point where τ_c of cohesive banks, which is rarely measured, becomes larger than τ_c of noncohesive bed sediments, on average. This corresponds roughly to the range of fluid entrainment stresses ($6 \leq \tau_c \leq 9 \text{ Pa}$) that we have measured in the laboratory for sand/kaolinite-clay mixtures (40 to 100% clay) (32) meant to represent cohesive riverbanks (Fig. 2A) (32). Similar to gravel-bedded rivers, we hypothesize that much of the scatter in the fine-grained rivers is related to site-specific variation in τ_c —although for the bank-toe material, rather than the bed. Next, we examine the distribution of fluid shear velocity, $U^* = \sqrt{\tau_{bf}/\rho}$, for flows exceeding bankfull. Phillips *et al.* (16) posited that maintenance of a stable average channel geometry requires that U^* values exceeding bankfull (U_{bf}^*) drop off rapidly, and showed for gravel-bedded rivers that this drop-off is exponential due to the massive increase in water discharge required to elevate fluid shear stresses beyond the confines of the channel. While U^* distributions for fine-grained rivers vary widely, normalizing each distribution by U_{bf}^* reveals a trend that is identical to gravel-bedded rivers (Fig. 2, B and C), for which $U_{bf}^* \approx 1.1 U_c^*$ (equivalent to $\tau_{bf} \approx 1.2 \tau_c$; i.e., the Parker closure). For the fine-grained rivers, we do not know the U_c^* of the cohesive and/or vegetated banks. If the threshold-limited channel model is correct, we may use the relation $U_{bf}^* \approx 1.1 U_c^*$ to infer that the range of entrainment stresses for bank materials is $3 \leq \tau_c \leq 10 \text{ Pa}$. These values are reasonable considering reported ranges for muddy riverbanks in the literature (23, 32, 43).

With this tentative support for the threshold-limited channel model, we test its ability to predict the width of all of the alluvial rivers in the global dataset, as a function of the imposed parameters slope and discharge. Predictive use of Eqs. 1 and 2 requires assuming values for C_f and τ_c . For gravel-bedded rivers ($D_{50} > 1 \text{ cm}$), we apply a constant $C_f = 8.69$ that is the average value of those channels (see the Supplementary Materials), while τ_c for each river is determined using the Shields curve (21). For fine-grained rivers ($D_{50} < 1 \text{ cm}$), where we assume that bank cohesion is limiting, we assign a constant $\tau_c = 8 \text{ Pa}$ that is representative of sand-clay mixtures (32), and an average $C_f = 11.12$. Modeled channel widths cluster around measured values (Fig. 2D) for the entire dataset, with fine-grained rivers plotting right on top of gravel-bedded rivers. This demonstrates that

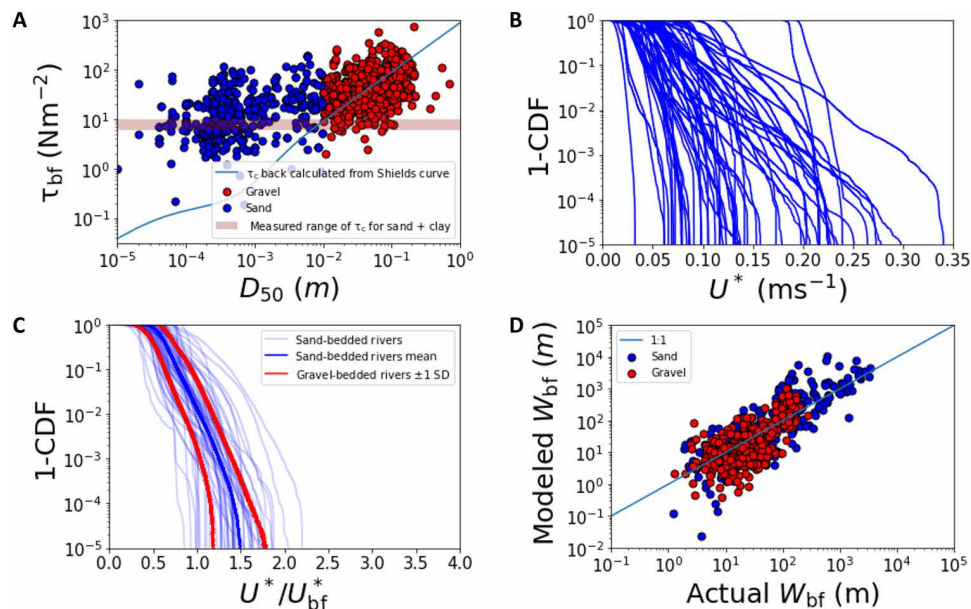


Fig. 2. Flow and geometry conditions for the global river data. (A) Bankfull shear stress τ_{bf} against median grain size D_{50} for gravel-bedded ($D > 1$ cm) and fine-grained ($D < 1$ cm) rivers. Blue line is τ_c determined from bed D_{50} based on the Shields curve (27). Pink band shows our experimentally determined range of τ_c for sand-clay mixtures (32). Note that gravel-bedded rivers generally follow the Shields curve indicating bed sediment control, while fine-grained rivers are consistent with cohesive bank control. (B) U^* magnitude-frequency distribution for a subset of fine-grained rivers in the global dataset ($n = 56$) showing high variability. (C) The same as (B) but normalized by U_{bf}^* for each river. Data collapse along a single curve; the dark blue line is the mean curve of fine-grained rivers, while red lines show SD of gravel-bedded rivers (16), which are nearly identical to the fine-grained dataset. (D) Modeled W_{bf} using Eq. 1 versus measured W_{bf} values for all rivers in the global dataset; τ_c for gravel-bedded rivers was computed from the Shields curve, and for sand-bedded rivers, we assumed a constant value of $\tau_c = \text{Pa}$ representative of cohesive banks. CDF, cumulative distribution function.

the first-order trend in channel hydraulic geometry may be predicted using the threshold-limited channel model, assuming a fixed threshold stress for fine-grained rivers.

We acknowledge here that the use of these regime equations with a fixed value for C_f is a drastic oversimplification of the many potential sources of momentum dissipation in natural channels (e.g., grains, bed forms, bars, meander bends). Changes in channel roughness can significantly alter the effective shear stress on the channel bed (44), and such roughness effects have been shown to have an influence on the geometry of river channels (31). Given the robust trend resultant from our simplified modeling (Fig. 2D), we do not consider variable channel roughness to be a first-order control on hydraulic geometry across all alluvial rivers. We suspect, however, that variation in channel roughness is an important contributing factor to the substantial scatter around the 1:1 line. We also acknowledge that the large scatter in the global dataset may be due to our general treatment of the variables in question as independent—and ignoring covariance that likely exists among them—as well as propagating unknown error through taking averages of random variables that are in themselves averages (e.g., the depth and slope components of the shear stress calculation). Last, the usage of general formulations such as the depth-slope product, for such a wide range of channels, can introduce additional error into the analysis by ignoring factors that might be influential in certain settings—such as the effects of wall drag in narrower channels. Nonetheless, despite the many potential sources for error, this treatment is common in many fluvial geomorphology studies; we follow this procedure due to the limited data available and to allow comparison to previous work.

Field case study

The global dataset provides several pieces of compelling, but indirect, evidence for the threshold-limited channel model. A direct test requires in situ measurement of the fluid entrainment threshold of bank-toe materials in a river with a sand bed and cohesive banks. Up to now, existing methods were either too unwieldy or too indirect to determine τ_c at targeted locations in a channel. We have developed a new instrument, the Mudbuster, that is specifically designed to overcome these shortcomings (32). The Mudbuster imposes an impeller-driven, rotational shear flow on an 18-cm diameter region of a riverbed or riverbank, and gradually increases the fluid shear stress until turbidity in the fluid column above the bed spikes, which is taken to be the entrainment threshold τ_c . The principle, design, calibration, and testing of the Mudbuster are reported elsewhere (32). Here, we report its first field deployment on the Mullica River, a sinuous and single-thread sand-bedded river ($D_{50} \approx 0.4$ mm; see Materials and Methods and fig. S4) with muddy banks, that is located in the Pine Barrens within the New Jersey coastal plain (Fig. 3). We selected a 150-m reach of the river ($Q_{bf} \approx 4.5 \text{ m}^3 \text{ s}^{-1}$, $S = 0.0008$, $W_{bf} \approx 5$ m, $H_{bf} \approx 1.2$ m; see Materials and Methods and fig. S5) in which vegetation rooting depths were shallow compared with channel depth, to isolate sediment cohesion effects that could be measured directly with the Mudbuster. We surveyed 18 channel cross sections spaced roughly one channel-width apart to determine τ_{bf} and measured τ_c of the bank-toe material at each station (see Materials and Methods). The average value $\tau_c = 4.5$ Pa for bank-toe material is over 10 times larger than τ_c for noncohesive sand [$\tau_c = 0.3$ Pa (32)]. We find that all 18 cross sections are close to $\tau_{bf} = 1.2\tau_c$ for the bank material, with no cross section showing a

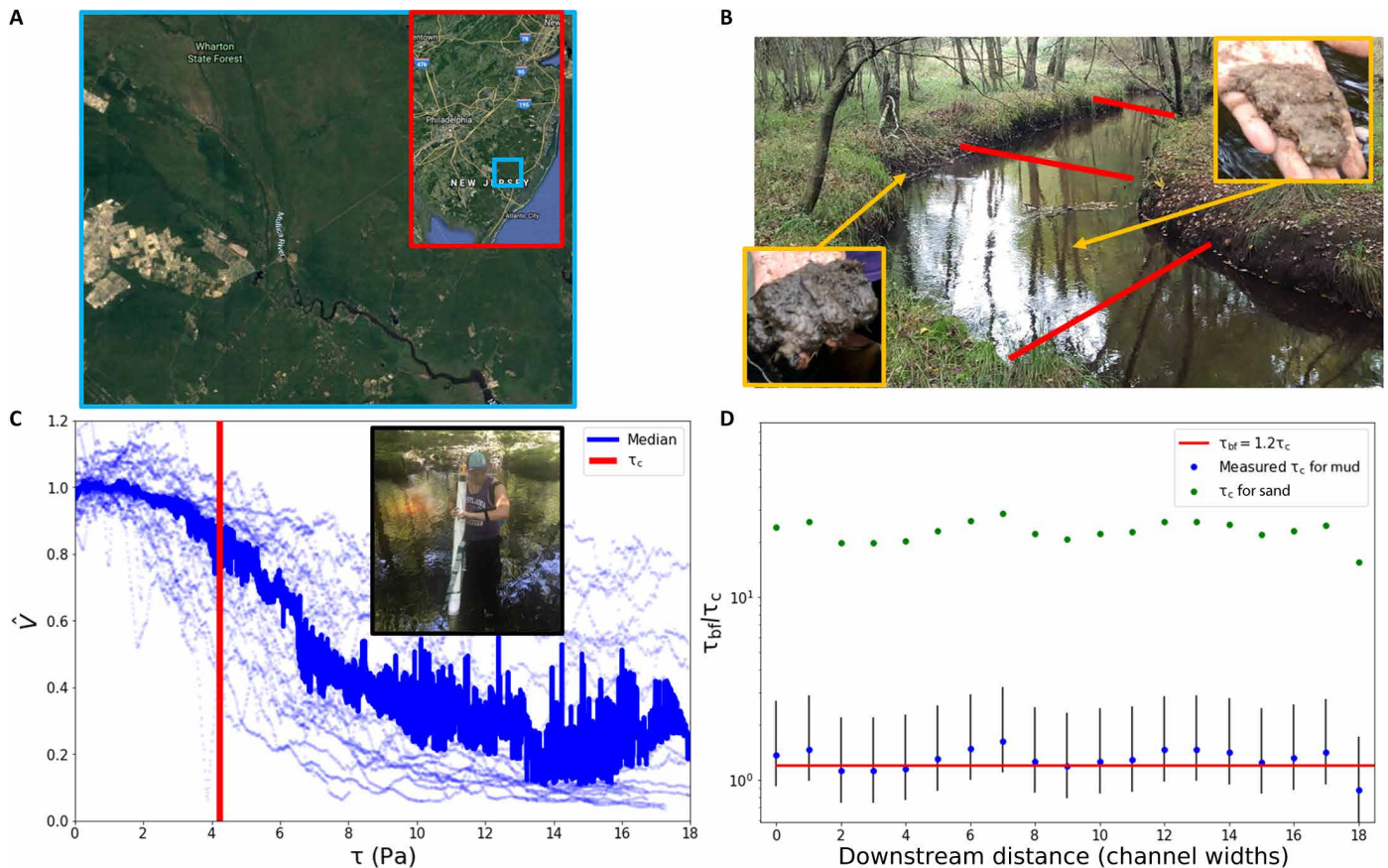


Fig. 3. Threshold-limited channel model case study. (A) Location of the Mullica river watershed in Wharton State Forest in the New Jersey coastal plain, with inset showing larger regional context (image source: Google Earth). (B) Portion of the surveyed reach of the Mullica River. Red lines mark surveyed cross sections. Muddy bank and bed materials are shown in the bottom left and top right, respectively. Photo credit: Kieran Dunne, Rice University. (C) Mudbuster measurements used to determine τ_c of bank-toe material. The fluid shear stress τ is gradually ramped up, while turbidity is measured as a voltage drop normalized by the initial voltage before shearing, \hat{V} (32). Thin blue lines show 28 independent measurements of bank-toe material, and solid line represents the median from those measurements; red line shows the mean value Pa determined from these data (see Materials and Methods). Inset: Implementation of the “Mudbuster” to measure τ_c of bank-toe material; device is controlled using a smart phone via a Bluetooth connection (32). Photo credit: Kieran Dunne, Rice University. (D) Values of τ_{bf}/τ_c for all 18 cross sections, where $\tau_c = 4.5$ Pa was determined from the average of bank-toe material measurements; the Parker model value $\tau_{bf}/\tau_c = 1.2$ is shown for reference, and error bars indicate ± 1 SD. Green points show $\tau_{bf}/\tau_c \gg 1$ for sand-bedded material, indicating control of cohesive bank-toe material on channel geometry.

bankfull shear stress larger than 1.5 times critical. These results confirm that, when the local entrainment threshold of cohesive banks is properly characterized (e.g., measured $\tau_c = 4.5$ Pa, instead of the assumed 8 Pa as used in Fig. 2D), the sand-bedded Mullica River is a near-threshold channel for the more resistant bank-toe material, but well above the threshold for the sand bed. We view this as a direct confirmation of the threshold-limited channel model.

Planform morphology

Because of the influence of τ_c on channel width (Eq. 1) and depth (Eq. 2), we anticipate that the most resistant material will exert a first-order control on channel planform morphology. Laboratory experiments examining self-formed sand rivers have induced a transition from braiding to single-thread channels, by enhancing bank strength through the addition of vegetation (9) and/or cohesive sediment (10). Braiding is associated with channels that have large aspect ratios, $W_{bf}/H_{bf} > 50$ (45). A scale analysis based on hydrodynamic considerations of bar formation (46) successfully predicts

the transition from single-threaded to multiple-threaded (braided) planform morphologies as a function of Q_{bf} , S , W_{bf} , and H_{bf} (47). Using our Eqs. 1 and 2, we recast this hydrodynamic criterion, ϵ , in terms of the threshold stress of the most resistant material, τ_c

$$\epsilon = \frac{Q_{bf} S^{5/2} g^2 \rho^{5/2}}{\pi C_f^2 (1.2 \tau_c)^{5/2}} \quad (3)$$

where we expect braiding for $\epsilon > 1$ and a single-thread morphology for $\epsilon < 1$ (46). Our global dataset is composed almost exclusively of U.S. Geological Survey gauging stations placed in single-threaded channels and should therefore plot overwhelmingly below the $\epsilon = 1$ plane in the phase space of the imposed variables Q_{bf} , S , and τ_c (Fig. 4C). We compute ϵ for all rivers (Eq. 3) using the Shields curve to determine τ_c and a fixed global average value $C_f = 9.74$ (minimal overall variation between gravel- and sand-bedded channels; fig. S1). Almost all of the gravel rivers (392 of 406) plot below the $\epsilon = 1$ plane; i.e., the expected morphology agrees with observations. In

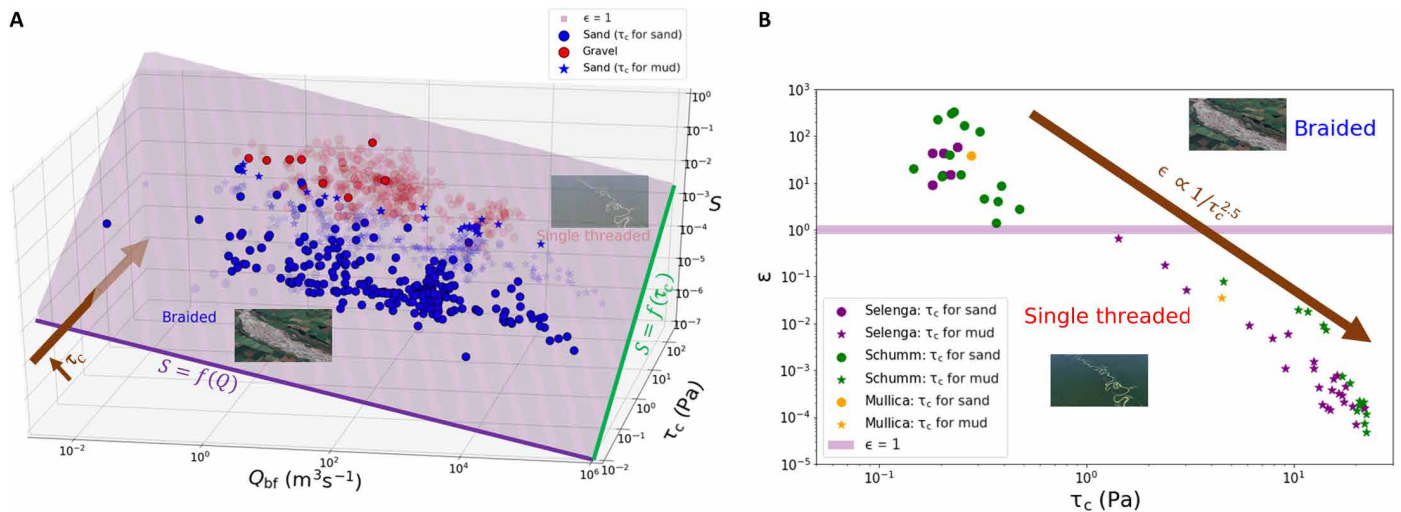


Fig. 4. Planform morphospace of alluvial rivers in the global dataset. (A) Global dataset: Hydrodynamic criterion $\epsilon = 1$ shown by the plane indicates the expected separation of braided from single-threaded channels in the parameter space of discharge Q_{bf} , slope S , and entrainment threshold τ_c . Inset images show typical braided morphology of the Waimakariri River, and single-threaded meandering Rio Purus (image sources: Google Earth). Virtually, all rivers in this dataset should plot as single threaded. When τ_c for bed sediment D_{50} determined from the Shields curve is used, gravel-bedded rivers almost invariably plot as single thread, but fine-grained rivers are mostly braided. Using a representative $\tau_c = 8$ Pa for mud instead, fine-grained rivers shift to the correct single-threaded morphospace. Purple line highlights $Q_{bf}-S$ relation for a given τ_c , which follows the classic empirical delineation (54). Green line indicates τ_c-S relations for a given Q_{bf} . Brown arrow shows how increasing τ_c can drive migration across the $\epsilon = 1$ plane. (B) Stability criterion ϵ computed from Eq. 3 as a function of τ_c for a set of single-threaded rivers with sand beds and muddy banks in which τ_c of bank-toe was measured (Mullica) or could be estimated from reported descriptions of bank material (49) (Schumm and Selenga). ϵ is computed using two different values for τ_c : the bed and bank materials. Selenga River delta channels were selected so as to be outside of the range of the backwater effect (48), and additional rivers were reported by Schumm (24). Brown arrow shows how increasing τ_c , by considering the threshold for more resistant bank (instead of bed) materials, can drive migration across the $\epsilon = 1$ plane.

contrast, most of the fine-grained rivers (264 of 305) plot above the $\epsilon = 1$ plane; i.e., the predicted braided morphology is not what is observed. Assuming a representative cohesive bank entrainment threshold of $\tau_c = 8$ Pa, however, shifts almost all of the fine-grained rivers (279 of 395) into the single-threaded regime—in compliance with their observed morphology. The assumption of a fixed τ_c for bank materials is, of course, a crude assumption. We find that improved knowledge of site-specific τ_c results in better predictions (Fig. 4B). We consider the case of the Mullica River where τ_c was directly measured, and some channels in the Selenga Delta (48) and several rivers studied by Schumm (22) where τ_c may be roughly estimated from reported silt and clay content using an empirical correlation function (49). All of these rivers are sand-bedded rivers with cohesive channel banks and plot well into the braided regime if τ_c for bed material is used. Fixing Q_{bf} and S for each river, but using τ_c for the more resistant bank material as opposed to τ_c for sand, we find that ϵ decreases and these rivers shift into the morphospace compliant with their observed morphology (Fig. 4B). These results provide an explanation for the observation that single-threaded, sand-bedded rivers in nature and the laboratory (9) seem to require cohesive and/or vegetated banks. Last, we suggest that the downstream transition from a gravel- to a sand-bedded river may lead to a shift from bed to bank control, which may explain downstream changes in planform morphology such as that seen on the Fraser River (fig. S2) (50).

DISCUSSION

Our findings indicate that average alluvial river geometry may be predicted with knowledge of four parameters: bankfull discharge,

slope, friction factor, and entrainment stress of the most resistant material. Although friction factor varies among rivers, this variation is not systematic with any other parameter (fig. S1) (23). More refined models for determining C_f may improve channel geometry predictions (31); to first order, however, one may assume $C_f \sim 10^1$. Improved knowledge of τ_c leads to more accurate predictions of bankfull width and depth, echoing other recent studies that have pointed out the need for site-specific measurements of threshold (16, 17). Results demonstrate that the Parker closure for gravel rivers can be extended to finer-grained systems by considering the most resistant (bank) material. This model can describe the average geometry of dynamic alluvial rivers in nature, including those that transport bed sediment at a stress state far above threshold. We assert that this mean field approximation is not at odds with dynamic equilibrium theories; rather, they are two sides of the same coin. To apply the mean field approximation, time-varying changes in τ_c of riverbank material, just like space-varying changes in fluid flow around meander bends, must be suitably averaged. For some engineering applications, use of such a large space- and time-averaged model may not be useful. With the addition of properly calibrated and site-specific estimates for τ_c and C_b , however, predictive power on the scale of engineering applications can be greatly improved—as demonstrated for the Mullica River case study. In many contexts, the additional information required to develop and apply models more sophisticated than the threshold-limiting channel model is simply not available. By using temporally and spatially averaged values for τ_c and τ_{bf} , we can build a simplified theory that is applicable for first-order predictions with limited information. This framework also illustrates how changing riverbank composition, as well as interactions with biological forcings (e.g., biofilms, tree roots)

that may influence bank stability, can induce a change in planform morphology from braiding to meandering, which has implications for interpreting alluvial river deposits on Earth and Mars (51, 52). The simple models Eqs. 1 and 2 may find immediate use in some applications, where management and restoration of river channels require an understanding of the relations between hydraulics and channel geometry. The apparent success of the threshold-limited channel model, however, raises other intriguing questions. This approach is purely hydraulic: Channel geometry is determined by the conveyance capacity of water (Q_{bf} , S , and C_f) and the entrainment threshold of the channel margins (τ_c). While sediment grain size influences τ_c , the sediment discharge supplied to the channel, Q_s , does not appear anywhere in this formulation. Sediment supply has been proposed to influence channel geometry (18) and also planform morphology (45). We posit that there is an influence of sediment supply through its modulation of slope. On engineering (decadal) time scales, slope is often considered an independent variable because its time scale of adjustment is much slower than width and depth (16, 53). Over longer time scales, however, threshold channel models indicate that $S \sim Q_s/Q_{bf}$ (26, 53). We suggest that changing sediment supply rate Q_s has a slow influence on channel geometry through regrading of river slope. If changes in supply influence grain size, however—either by changing the size fed to channels or by inducing armoring of the riverbed (18, 53)—then they will have a more direct and immediate impact on geometry by altering τ_c .

MATERIALS AND METHODS

We used Google Earth's ruler tool to collect measurements of W_{bf} for the Lochsa River. Images of the channel were not necessarily taken at bankfull conditions, so bankfull extent was estimated on the basis of color variations with an approximate pixel resolution of 0.65 m. Measurements of Q_{bf} , S , D_{50} , and τ_c for the Lochsa River were reported in the supplementary materials of Phillips *et al.* (16). The global dataset we used has been presented elsewhere (23). It contains measured channel geometry and discharge values associated with bankfull flow, i.e., when the channel is completely filled with water. Friction factor C_f for each river was computed using a Darcy-Weisbach flow resistance relation (Supplementary Materials). Estimates for the threshold entrainment stress (τ_c) of noncohesive sediment were determined from an empirical fit to the Shields curve (21), which represents the combined fluid drag and lift forces required to overcome particle friction. Channel geometry and bank composition data for rivers presented in Fig. 4B were taken from reported values in the associated publications (22, 48). Estimates of threshold entrainment stress for cohesive sediment in these additional rivers were calculated using an empirical relation between τ_c and percentage of silt-clay (49).

Data to produce the hydrograph magnitude-frequency curves (Fig. 2, B and C) were collected from the U.S. Geological Survey (USGS) website and analyzed using code and methodology developed by Phillips *et al.* (16). Gravel-bedded rivers were the same rivers analyzed by Phillips *et al.* (16); we added fine-grained rivers from a global dataset (23) for which sufficient data were available. Because of heavy overlap between the gravel- and fine-grained rivers, only the mean for fine-grained rivers and SD for gravel-bedded rivers are shown.

The Mullica River was selected for field work because of its proximity and the desired bed and bank properties for the study. Channel slope for the studied reach was determined over a 6-km stretch of

river using a Trimble ProXH differential GPS sampling at 1 Hz from a boat (fig. S3). Bed grain size was relatively uniform throughout the reach and was measured using a CAMSIZER (fig. S4). We surveyed bankfull channel width and depth at 18 cross sections using a laser range finder (fig. S5). Calculations of bankfull stress at each location used the bankfull depth at each cross section and the reach-averaged slope. At each cross section, the edge of the bank was identified in the field. Bank-toe erodibility measurements were made using the Mudbuster in situ erodibility tester following the procedures and calibrations outlined in another paper (32). At each cross section, four measurements of τ_c were taken at the toe of the channel bank. Fluid shear stress is systematically increased with the Mudbuster, while turbidity is measured using two photodiodes. Increased turbidity measures as a voltage drop, which is expected to occur abruptly at a threshold fluid stress. While each measurement showed a voltage decline with increasing applied shear stress, determining a precise threshold was challenging due to noise. Variations of the voltage drop from measurements within a single cross section and measurements among different cross sections were of comparable magnitude. Accordingly, we lumped together all voltage drop curves to produce a more robust statistical determination of the average τ_c for all cross sections (Fig. 3). This is the reach-averaged value $\tau_c = 4.5$ Pa reported in the text.

SUPPLEMENTARY MATERIALS

Supplementary material for this article is available at <http://advances.sciencemag.org/cgi/content/full/6/41/eabc1505/DC1>

REFERENCES AND NOTES

- N. R. Council, *Landscapes on the Edge: New Horizons for Research on Earth's Surface* (National Academies Press, 2010).
- D. R. Montgomery, W. E. Dietrich, Where do channels begin? *Nature* **336**, 232–234 (1988).
- N. Izumi, G. Parker, Linear stability analysis of channel inception: Downstream-driven theory. *J. Fluid Mech.* **419**, 239–262 (2000).
- F. Métivier, E. Lajeunesse, O. Devauchelle, Laboratory rivers: Lacey's law, threshold theory, and channel stability. *Earth Surf. Dyn.* **5**, 187–198 (2017).
- G. Lacey, *Minutes of the Proceedings of the Institution of Civil Engineers* (Thomas Telford-ICE Virtual Library, 1930), vol. 229, pp. 259–292.
- G. Parker, Self-formed straight rivers with equilibrium banks and mobile bed. part 2. The gravel river. *J. Fluid Mech.* **89**, 127–146 (1978).
- M. Church, Bed material transport and the morphology of alluvial river channels. *Annu. Rev. Earth Planet. Sci.* **34**, 325–354 (2006).
- S. A. Schumm, H. R. Khan, Experimental study of channel patterns. *Geol. Soc. Am. Bull.* **83**, 1755–1770 (1972).
- M. Tal, C. Paola, Dynamic single-thread channels maintained by the interaction of flow and vegetation. *Geology* **35**, 347–350 (2007).
- C. A. Braudrick, W. E. Dietrich, G. T. Leverich, L. S. Sklar, Experimental evidence for the conditions necessary to sustain meandering in coarse-bedded rivers. *Proc. Natl. Acad. Sci. U.S.A.* **106**, 16936–16941 (2009).
- J. Pitlick, J. Marr, J. Pizzuto, Width adjustment in experimental gravel-bed channels in response to overbank flows. *J. Geophys. Res. Earth* **118**, 553–570 (2013).
- L. B. Leopold, T. Maddock, *The Hydraulic Geometry of Stream Channels and Some Physiographic Implications* (US Government Printing Office, 1953), vol. 52.
- G. P. Williams, Bank-full discharge of rivers. *Water Resour. Res.* **14**, 1141–1154 (1978).
- A. Blom, L. Arkesteijn, V. Chavarrias, E. Viparelli, The equilibrium alluvial river under variable flow and its channel-forming discharge. *J. Geophys. Res. Earth* **122**, 1924–1948 (2017).
- M. G. Wolman, J. P. Miller, Magnitude and frequency of forces in geomorphic processes. *J. Geol.* **68**, 54–74 (1960).
- C. B. Phillips, D. J. Jerolmack, Self-organization of river channels as a critical filter on climate signals. *Science* **352**, 694–697 (2016).
- C. B. Phillips, D. J. Jerolmack, Bankfull transport capacity and the threshold of motion in coarse-grained rivers. *Water Resour. Res.* **55**, 11316–11330 (2019).
- A. M. Pfeiffer, N. J. Finnegan, J. K. Willenbring, Sediment supply controls equilibrium channel geometry in gravel rivers. *Proc. Natl. Acad. Sci. U.S.A.* **114**, 3346–3351 (2017).

19. B. C. Eaton, M. Church, Predicting downstream hydraulic geometry: A test of rational regime theory. *J. Geophys. Res. Earth* **112**, F03025 (2007).
20. R. G. Millar, M. C. Quirk, Stable width and depth of gravel-bed rivers with cohesive banks. *J. Hydraul. Eng.* **124**, 1005–1013 (1998).
21. L. C. van Rijn, Initiation of motion and suspension; critical bed-shear stress for sand-mud mixtures (2016).
22. S. A. Schumm, The shape of alluvial channels in relation to sediment type. USGS Professional Paper (1960).
23. K. B. J. Dunne, D. J. Jerolmack, Evidence of, and a proposed explanation for, bimodal transport states in alluvial rivers. *Earth Surf. Dyn.* **6**, 583–594 (2018).
24. S. A. Schumm, Sinuosity of alluvial rivers on the great plains. *Geol. Soc. Am. Bull.* **74**, 1089–1100 (1963).
25. M. Kleinhans, W. van Dijk, W. van de Lageweg, R. Hoendervoogt, H. Markies, F. Schuurman, From nature to lab: scaling self-formed meandering and braided rivers, in *River Flow 2010*, A. Ditttrich, Ka. Koll, J. Aberle, P. Geisenhainer, Eds. (Karlsruhe, 2010), vol. 2, pp. 1001–1010.
26. G. Parker, Self-formed straight rivers with equilibrium banks and mobile bed. part 1. The sand-silt river. *J. Fluid Mech.* **89**, 109–125 (1978).
27. S. Ikeda, N. Izumi, Stable channel cross sections of straight sand rivers. *Water Resour. Res.* **27**, 2429–2438 (1991).
28. C. Li, M. J. Czapiga, E. C. Eke, E. Viparelli, G. Parker, Variable shields number model for river bankfull geometry: Bankfull shear velocity is viscosity-dependent but grain size-independent. *J. Hydraul. Res.* **53**, 36–48 (2015).
29. K. Gaurav, F. Métivier, O. Devauchelle, R. Sinha, H. Chauvet, M. Houssais, H. Bouquerel, Morphology of the kosi megafan channels. *Earth Surf. Dyn.* **3**, 321–331 (2015).
30. O. Devauchelle, A. P. Petroff, A. E. Lobkovsky, D. H. Rothman, Longitudinal profile of channels cut by springs. *J. Fluid Mech.* **667**, 38–47 (2011).
31. S. Francalanci, S. Lanzoni, L. Solari, A. N. Papanicolaou, Equilibrium cross-section of river channels with cohesive erodible banks. *J. Geophys. Res. Earth* **125**, e2019JF005286 (2020).
32. K. Dunne, P. Arratia, D. Jerolmack, A new method for in-situ measurement of the erosion threshold of river channels (EarthArXiv, 2019).
33. E. Eke, G. Parker, Y. Shimizu, Numerical modeling of erosional and depositional bank processes in migrating river bends with self-formed width: Morphodynamics of bar push and bank pull. *J. Geophys. Res. Earth* **119**, 1455–1483 (2014).
34. K. Naito, G. Parker, Can bankfull discharge and bankfull channel characteristics of an alluvial meandering river be cospecified from a flow duration curve? *J. Geophys. Res. Earth* **124**, 2381–2401 (2019).
35. G. Parker, P. R. Wilcock, C. Paola, W. E. Dietrich, J. Pitlick, Physical basis for quasi-universal relations describing bankfull hydraulic geometry of single-thread gravel bed rivers. *J. Geophys. Res. Earth* **112**, F04005 (2007).
36. G. Parker, Y. Shimizu, G. V. Wilkerson, E. C. Eke, J. D. Abad, J. Lauer, C. Paola, W. E. Dietrich, V. R. Voller, A new framework for modeling the migration of meandering rivers. *Earth Surf. Process. Landf.* **36**, 70–86 (2011).
37. W. E. Dietrich, J. D. Smith, T. Dunne, Flow and sediment transport in a sand bedded meander. *J. Geol.* **87**, 305–315 (1979).
38. D. J. Furbish, River-bend curvature and migration: How are they related? *Geology* **16**, 752–755 (1988).
39. J. A. Clayton, J. Pitlick, Spatial and temporal variations in bed load transport intensity in a gravel bed river bend. *Water Resour. Res.* **43**, W02426 (2007).
40. L. P. Kadanoff, More is the same; phase transitions and mean field theories. *J. Stat. Phys.* **137**, 777 (2009).
41. E. C. Eke, M. J. Czapiga, E. Viparelli, Y. Shimizu, J. Imran, T. Sun, G. Parker, Coevolution of width and sinuosity in meandering rivers. *J. Fluid Mech.* **760**, 127–174 (2014).
42. S. M. Trampus, S. Huzurbazar, B. McElroy, Empirical assessment of theory for bankfull characteristics of alluvial channels. *Water Resour. Res.* **50**, 9211–9220 (2014).
43. G. J. Hanson, A. Simon, Erodibility of cohesive streambeds in the loess area of the midwestern usa. *Hydrol. Process.* **15**, 23–38 (2001).
44. J. W. Kean, J. D. Smith, Form drag in rivers due to small-scale natural topographic features: 1. regular sequences. *J. Geophys. Res. Earth* **111**, F04009 (2006).
45. B. C. Eaton, R. G. Millar, S. Davidson, Channel patterns: Braided, anabranching, and single-thread. *Geomorphology* **120**, 353–364 (2010).
46. G. Parker, On the cause and characteristic scales of meandering and braiding in rivers. *J. Fluid Mech.* **76**, 457–480 (1976).
47. D. J. Jerolmack, D. Mohrig, Conditions for branching in depositional rivers. *Geology* **35**, 463–466 (2007).
48. T. Y. Dong, J. A. Nittrouer, M. J. Czapiga, H. Ma, B. McElroy, E. Il'icheva, M. Pavlov, S. Chalov, G. Parker, Roles of bank material in setting bankfull hydraulic geometry as informed by the selenga river delta, russia. *Water Resour. Res.* **55**, 827–846 (2019).
49. J. P. Julian, R. Torres, Hydraulic erosion of cohesive riverbanks. *Geomorphology* **76**, 193–206 (2006).
50. J. G. Venditti, M. Church, Morphology and controls on the position of a gravel-sand transition: Fraser river, british columbia. *J. Geophys. Res. Earth* **119**, 1959–1976 (2014).
51. V. Ganti, A. C. Whittaker, M. P. Lamb, W. W. Fischer, Low-gradient, single-threaded rivers prior to greening of the continents. *Proc. Natl. Acad. Sci. U.S.A.* **116**, 11652–11657 (2019).
52. A. Ielpi, M. G. A. Lapôte, A tenfold slowdown in river meander migration driven by plant life. *Nat. Geosci.* **13**, 82–86 (2020).
53. C. Paola, G. Parker, R. Seal, S. K. Sinha, J. B. Southard, P. R. Wilcock, Downstream fining by selective deposition in a laboratory flume. *Science* **258**, 1757–1760 (1992).
54. L. B. Leopold, M. G. Wolman, *River Channel Patterns: Braided, Meandering, and Straight* (US Government Printing Office, 1957).

Acknowledgments: We thank J. Pizzuto, J. Nittrouer, and C. Phillips for initial feedback that helped frame aspects of this paper, and D. Furbish, G. Parker, and an anonymous reviewer for comments that improved the clarity and rigor of the manuscript. We thank C. Phillips for sharing hydrograph analysis code. We thank Q. Zhang and J. Seok for assistance in carrying out the field investigation. **Funding:** The research was sponsored by the Army Research Laboratory and the National Science Foundation and was accomplished under grant numbers W911-NF-16-1-0290 and 1734355, respectively. **Author contributions:** K.B.J.D. performed the research and analyzed the data, D.J.J. supervised the research, and both authors wrote the paper. **Competing interests:** The authors declare that they have no competing financial interests. **Data and materials availability:** All data generated during this study are displayed in the Supplementary information files and available for download at this OSF data repository: <https://osf.io/j7xn6/>. All data needed to evaluate the conclusions in the paper are present in the paper and/or the Supplementary Materials. Additional data related to this paper may be requested from the authors.

Submitted 8 April 2020
 Accepted 24 August 2020
 Published 7 October 2020
 10.1126/sciadv.abc1505

Citation: K. B. J. Dunne, D. J. Jerolmack, What sets river width? *Sci. Adv.* **6**, eabc1505 (2020).

What sets river width?

Kieran B. J. Dunne and Douglas J. Jerolmack

Sci Adv **6** (41), eabc1505.
DOI: 10.1126/sciadv.abc1505

ARTICLE TOOLS

<http://advances.sciencemag.org/content/6/41/eabc1505>

SUPPLEMENTARY MATERIALS

<http://advances.sciencemag.org/content/suppl/2020/10/05/6.41.eabc1505.DC1>

REFERENCES

This article cites 46 articles, 10 of which you can access for free
<http://advances.sciencemag.org/content/6/41/eabc1505#BIBL>

PERMISSIONS

<http://www.sciencemag.org/help/reprints-and-permissions>

Use of this article is subject to the [Terms of Service](#)

Science Advances (ISSN 2375-2548) is published by the American Association for the Advancement of Science, 1200 New York Avenue NW, Washington, DC 20005. The title *Science Advances* is a registered trademark of AAAS.

Copyright © 2020 The Authors, some rights reserved; exclusive licensee American Association for the Advancement of Science. No claim to original U.S. Government Works. Distributed under a Creative Commons Attribution NonCommercial License 4.0 (CC BY-NC).